Four-wave-mixing imaging and carrier dynamics of PbS colloidal quantum dots

Francesco Masia,[1,2,*] Iwan Moreels,[3] Zeger Hens,[3] Wolfgang Langbein,[2] and Paola Borri[1]
[1]*School of Biosciences, Cardiff University, Museum Avenue, Cardiff CF10 3AX, United Kingdom*
[2]*School of Physics and Astronomy, Cardiff University, The Parade, Cardiff CF24 3AA, United Kingdom*
[3]*Department of Inorganic and Physical Chemistry, Ghent University, Krijgslaan 281-S3, Ghent B-9000, Belgium*
(Received 27 July 2010; revised manuscript received 3 September 2010; published 1 October 2010)

We demonstrate coherent multiphoton imaging of PbS colloidal quantum dots based on the detection of their transient resonant four-wave-mixing (FWM) emission under 150 fs pulsed laser excitation. Background-free imaging of PbS quantum dots in resonance with their ground-state excitonic absorption at 1.2 μm wavelength is shown, with intrinsic optical sectioning and a spatial resolution better than the one-photon diffraction limit, promising for deep tissue microscopy. The four-wave-mixing efficiency is found to be resonant to the ground-state absorption maximum, which is a prerequisite for spectral multiplexing. The measured FWM dynamics is consistent with the presence of charged exciton and biexiton Auger recombination in the 10–100 ps time scale, phonon-assisted exciton thermalization in the nanosecond time scale, and excitonic recombination in the microsecond time scale.

DOI: 10.1103/PhysRevB.82.155302 PACS number(s): 78.67.Bf, 78.47.nj, 78.47.J−

I. INTRODUCTION

Semiconductor quantum dots have been widely investigated in recent years due to the possibility of tailoring their atomlike electronic energy levels by changing their size, composition, and shape, with exciting perspectives in photonics,[1] optoelectronics,[2] and for biological applications.[3] In particular, in the area of biolabeling and fluorescence microscopy, colloidal quantum dots (CQDs) were shown to exhibit superior photostability[4] and a larger multiphoton absorption cross section[5] than organic fluorophores.

Lead chalcogenide CQDs (PbX with X=S or Se) have a fundamental exciton absorption peak which can be wavelength tuned from ~700 nm to 3 μm.[6–10] The near-infrared wavelength window is desirable for imaging thick samples since infrared wavelength undergoes less Rayleigh scattering than visible light. Moreover, biological specimens have their weakest absorption in the 0.7–1.3 μm wavelength range, the near-infrared window in biological tissue. However, fluorescence imaging at wavelengths above 1 μm is limited by the high noise level of available detectors.

We recently demonstrated that, beyond fluorescence, CdSe/ZnS CQDs can be used for multiphoton microscopy by exploiting their third-order optical nonlinearity, resulting in four-wave mixing (FWM), when excited in resonance with their fundamental excitonic transition.[11,12] We showed that FWM imaging has intrinsic optical sectioning capabilities and that its spatial resolution supersedes the one-photon diffraction limit, owing to the nonlinearity of the signal. Importantly, FWM detection is performed interferometrically in a heterodyne scheme, which due to the large heterodyne gain provided by the reference field overcomes the problem of detector noise and can be shot-noise limited. FWM imaging is therefore ideally suited to perform multiphoton microscopy in the near infrared with PbS CQDs. The recently developed stimulated emission microscopy[13] uses a similar transmission modulation to image nonfluorescent chromophores.

Beyond imaging applications, PbX CQDs are also interesting from a fundamental physics point of view since the effective masses of electrons and holes are very similar and relatively small. The exciton Bohr radius is thus rather large (46 nm for PbSe and 18 nm for PbS) compared to the typical CQD sizes, and PbX CQDs can be considered as a model system for CQDs with strong confinement. Their band structure is different from the commonly investigated CdSe or InAs systems. Both the maximum of the valence band and the minimum of the conduction band are at the L points of the Brillouin zone. Therefore, the ground-state exciton is 64-fold degenerate, compared to the eightfold degeneracy of excitons in CdSe CQDs with a direct band gap at the Γ point.[14]

Owing to the strong quantum confinement, significant carrier-carrier Coulomb interaction and, in particular, Auger recombination is expected in PbX CQDs. Strong carrier-carrier scattering can also result in the generation of multiexcitons by a single high-energy photon, an effect known as carrier multiplication (CM) or multiexciton generation, which can be understood as the reverse of Auger recombination.[15,16] CM in PbX CQDs has generated much interested for its potential application in solar-energy conversion and photovoltaics devices but has been controversially discussed in the literature. After earlier reports of quantum efficiencies up to 700%,[15,17,18] recent measurements showed that no enhancement of the CM efficiency is observed in CQDs relatively to the bulk value.[16,19,20] This discrepancy has been attributed[16] to photoinduced charging of the CQDs giving rise to fast recombination dynamics similar to that of multiexcitons after CM.

With the focus on measuring carrier multiplication[15–18,21–23] and Auger recombination,[24–27] many recent experiments on carrier dynamics in PbX CQDs have been based on resolving the transient absorption bleaching of the excitonic ground-state transition after pulsed excitation at high photon energies. From these nonresonant pump-probe experiments, it is however difficult to extract the dynamics of the ground-state exciton only since many pathways come into play over similar time scales including carrier relaxation, photoionization, Auger recombination, and exciton redistribution between different energy states.

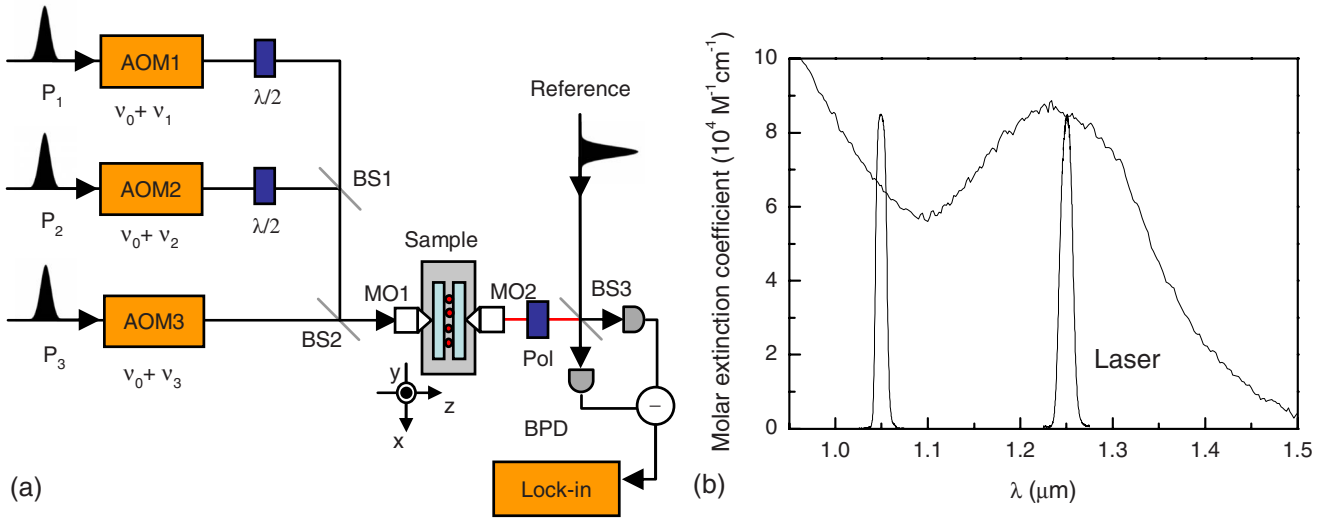

FIG. 1. (Color online) (a) Sketch of the experimental setup. AOM: Acousto-optic modulator. λ/2: wave plate. Pol: polarizer. *xyz*: Piezoelectric scanning stage. BS: 50:50 beam splitter. MO: microscope objective. BPD: balanced photodiodes. (b) Molar extinction coefficient spectrum of the 4.4 nm PbS CQDs, measured in C_2Cl_4. Also shown are spectral profiles of the laser pulses centered at 1.25 or 1.05 μm.

Transient degenerate FWM in a three-beam geometry is a known method to directly measure the excitonic population dynamics with pump and probe pulses both resonant to the same transition, as also recently demonstrated by us on InAs/GaAs quantum dots.[28] In the present work, we demonstrate near-infrared FWM imaging with PbS CQDs using a three-beam geometry, exploiting both the intensity and the lifetime of the FWM signal, and we use FWM to directly measure the ground-state exciton dynamics in a resonant pump-probe scheme.

II. SAMPLES AND EXPERIMENTS

A. CQD synthesis and sample preparation

The PbS CQD synthesis is based on the procedure of Cademartiri *et al.*,[9] and is described in detail in Ref. 29. The synthesis and subsequent ligand exchange yields oleic acid capped PbS CQDs, suspended in toluene. Their size and concentration in suspension are determined from the CQD absorbance spectrum, using a known sizing curve and molar extinction coefficient.[29] PbS/CdS CQDs are synthesized by a cation exchange reaction.[30] The synthesis is similar to the procedure described previously to prepare PbSe/CdSe and PbTe/CdTe CQDs.[31] For the FWM experiments, we used 4.4 nm PbS CQDs (fundamental exciton energy of E_0 =0.99 eV, equivalent to a first absorption peak at a wavelength of λ=1.25 μm). The effect of a CdS shell on the carrier dynamics was investigated by comparing core-only 4.6 nm PbS CQDs (E_0=0.96 eV, λ=1.29 μm) and 4.8 nm PbS/CdS core/shell CQDs with a shell thickness of 0.45 nm (E_0=0.94 eV, λ=1.32 μm). A small amount of CQDs is mixed with a solution of 10 mol % polystyrene in toluene, resulting in a 20 μM suspension. This is spin coated on a 0.17-mm-thick glass coverslip at a speed of 1000 rpm. A transmittance spectrum of the resulting thin film shows a distinct interference pattern, similar to results published recently,[32] suggesting macroscopic homogeneity of the dispersed PbS CQDs and a uniform film thickness of ~2 μm (when assuming a polystyrene refractive index of 1.6).

B. FWM generation

A schematic of the experimental setup used is shown in Fig. 1. Fourier-limited laser pulses of 150 fs duration (~17 nm spectral width) and tunable central wavelength at 76 MHz repetition rate are provided by an optical parametric oscillator pumped by a Ti:Sapphire laser. The pulse train is divided into four beams called reference, P_1, P_2, and P_3. The optical frequencies of pulses $P_{1,2,3}$ are upshifted by acousto-optic modulators driven at different radio frequencies. The delay time (τ_{12}) between the pulses P_1 and P_2 and between the pulses P_2 and P_3 (τ_{23}) can be controlled with ~20 fs temporal resolution using delay lines.

$P_{1,2,3}$ are subsequently recombined into the same spatial mode, and focused onto the sample by an oil-immersion microscope objective with 1.25 numerical aperture (80% transmittance at 1.2 μm) to achieve high spatial resolution. The sample can be moved with respect to the focal region of the objectives by a *xyz* piezoelectric scanning unit with nanometric resolution (Physik Instrumente PI F-130). The transmitted fields of $P_{1,2,3}$ and the nonlinear FWM field are collected by a second microscope objective, and their interference with the reference beam is detected by a pair of balanced InGaAs photodiodes (Hamamatsu G8376-03) and a lock-in amplifier (SRS 844). The transmitted beams and the emitted FWM signal can be distinguished by selecting the proper beating frequency in our heterodyne detection scheme, as discussed in detail in our previous works.[33,34] A cross-polarization scheme is used to reject background originating from nonlinearities of the photodiodes: the polarization states of $P_{1,2}$ are adjusted by a combination of $\lambda/4$ and $\lambda/2$ waveplates. $P_{1,2}$ are cross polarized with respect to the

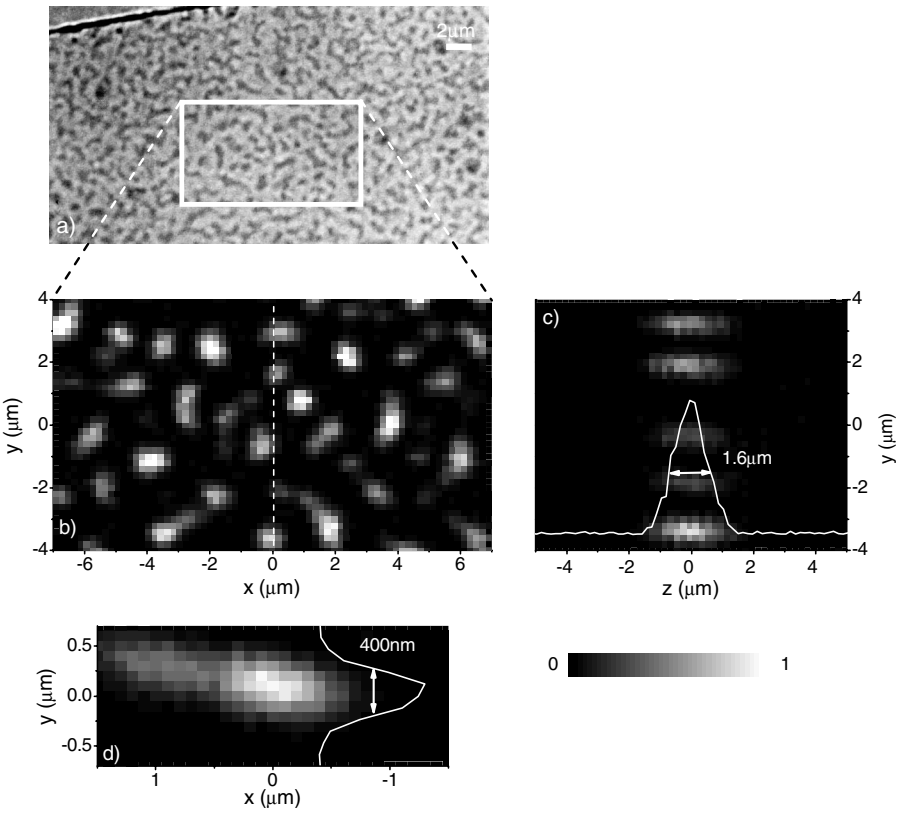

FIG. 2. (a) Bright-field image of PbS CQDs dispersed in a polystyrene film acquired with a 100× 1.3 *NA* oil-immersion microscope objective. (b)–(d) Resonant FWM microscopy of the sample. (b) FWM intensity as a function of the transverse x,y position of the sample. (c) yz scan of the FWM intensity at a fixed x position indicated by the dashed line in (b), pixel size 0.2 μm. (d) High-resolution xy scan (pixel size 0.1 μm). The white lines in panels (c) and (d) represent intensity profiles along the z and y direction, respectively. The excitation wavelength is 1.25 μm and the time-averaged excitation intensity in the focus is 5.5 kW/cm^2 (24 μJ/cm^2 per pulse) created by 17 μW average power. Linear grayscale. Time/pixel=30 ms.

reference, to minimize interference in the photodiodes, while the polarization of P_3 is equal to the reference field to maximize the detected FWM signal. All the experiments are performed at room temperature.

The FWM signal generation in this degenerate three-beam experiment resonant to the excitonic transition in CQDs can be sketched as follows. The field of the first pulse P_1 in resonance with an optical transition in the sample [see Fig. 1(b)] creates a coherent polarization. When the second resonant pulse P_2 delayed by τ_{12} arrives before the loss of polarization coherence (i.e., if τ_{12} is shorter than the dephasing time), a density modulation (over the pulse repetitions) is induced in the sample through the interference of the polarization with the second pulse, which in turn modulates the absorption, mainly due to phase-space filling nonlinearity.[35] The measured FWM field is due to the modulation of the transmitted P_3 by the absorption modulation. Changing the delay τ_{23} between P_2 and P_3, the dynamics of the optically induced modulated carrier density can be investigated.

Maximum FWM signal was found for pulses P_1 and P_2 in time overlap ($\tau_{12}=0$), which shows that the dephasing time of the exciton transition is shorter than the pulse width at this temperature in agreement with previous calculations and measurements.[6,36] The third pulse instead was delayed by $\tau_{23}=0.5$ ps, i.e., just after completion of the carrier density creation by $P_{1,2}$. These settings were used in all the imaging experiments, unless stated otherwise.

C. PSF calculation

The one-photon diffraction limit in the transversal direction is calculated using the full width at half maximum (FWHM) of the intensity distribution [point-spread function (PSF)] $I_t=[2J_1(v)/v]^2$, where J_1 is the first-order Bessel function and $v=2\pi xNA/\lambda$ with *NA* being the objective numerical aperture and λ the excitation wavelength. The one-photon diffraction limit in the axial direction is calculated using the FWHM of the intensity distribution $I_a=[\sin(u/4)/(u/4)]^2$, where $u=2\pi z(NA)^2/(\lambda n)$ (with $n=1.51$ refractive index of oil). For the FWM process the point-spread function is calculated as the fourth power of the one-photon intensity distribution, and the resolution is taken as the FWHM of the corresponding profile. This treatment of the PSF is valid for a pointlike emitter of size much smaller than the wavelength. For an extended object, the intensity PSF is not well defined due to the coherent nature of the signal, and the effective PSF can be up to a factor $\sqrt{2}$ wider.[37]

III. RESULTS AND DISCUSSION

A. Imaging

The imaging capabilities of resonant FWM microscopy are shown in Fig. 2. A sample was prepared by dispersing 4.4 nm PbS CQDs (fundamental exciton energy of 0.99 eV, equivalent to a first absorption peak at a wavelength of 1.25 μm) in a polymer film (see Sec. II A) and appeared macroscopically homogeneous. The bright-field image of the sample acquired with a 100× objective in visible light showed the presence of CQD agglomerates with a typical size of 0.5 μm [see Fig. 2(a)]. These agglomerates were imaged with FWM resonant at 1.25 μm, as shown in Fig. 2(b), revealing the absence of background in this contrast modality. The nonlinear nature of the FWM signal provides

intrinsic optical sectioning and improved spatial resolution beyond the one-photon diffraction limit. This is demonstrated in Fig. 2(c) showing a *yz* scan of the FWM intensity acquired along a fixed *x* position, as indicated by the dashed line in Fig. 2(b). The axial profile along a cluster has a FWHM of 1.6 μm, which is smaller than the one-photon diffraction limit of 2.2 μm calculated for this wavelength and the numerical aperture of the microscope objective (see Sec. II C). Similarly for the transverse resolution, we observed a cluster with a FWHM of 400 nm [see Fig. 2(d)], below the one-photon diffraction limit of 510 nm. Note that the measured FWHM represent *upper limits* of the resolution since the size of the CQD agglomerates is not known. Theoretically, due to the third-order FWM nonlinearity and confocal detection, a spatial resolution of 260 nm and 1.1 μm is expected in the transversal and axial direction, respectively (see Sec. II C). The improvement of a factor of 2 compared to the one-photon diffraction limit can be understood approximating the one-photon point-spread function (PSF_{1p}) by a Gaussian. The point-spread function of a multiphoton signal (PSF_{np}) can be calculated as $PSF_{np}=(PSF_{1p})^n$, where n is the field power creating the signal. The FWHM of the nth power of a Gaussian is reduced by a factor of $1/\sqrt{n}$. For the detected FWM signal $n=4$, considering the three exciting fields and the emitted field measured confocally, through the interference with the mode-matched reference field.

In order to quantify the sensitivity limit of the technique, we have studied the dependence of the FWM signal on the excitation intensity. The FWM amplitude at low excitation intensities is found to be proportional to the amplitudes of the optical fields of each of the three pulses, as expected from a third-order nonlinearity. As the excitation intensity increases, a deviation from the third-order behavior is observed, and eventually the signal saturates. In Fig. 3, the dependence of the FWM amplitude on the intensity of P_1 is shown. For equal excitation intensities of the three fields (triangles), we observed a deviation from the third-order regime (dashed line) for a total excitation intensity $I_{tot}=I_1+I_2+I_3$ above 20 kW/cm^2 (0.09 mJ/cm^2 per pulse per beam). Keeping P_3 at 30 kW/cm^2 (0.39 mJ/cm^2 per pulse) and varying the intensities of P_1 and P_2 (squares), the saturation of the signal occurs at $I_{tot}\sim 150$ kW/cm^2. Such intensities are compatible with live cell imaging, as demonstrated in viability studies of mammalian embryos imaged with two-photon fluorescence microscopy.[38] From the maximum emitted FWM signal at saturation, we have estimated the sensitivity limit of the technique. The number of quantum dots in the focal volume ($\sim 10^5$ CQDs) was inferred from the measured transmission and molar extinction coefficient [Fig. 1(b)]. The FWM field amplitude is proportional to the number of dots in the focal volume, and we found that the detection shot noise is equal to the saturated FWM signal from 100 CQDs per $\sqrt{\text{Hz}}$ detection bandwidth, corresponding to a volume fraction of 10^{-6} or a concentration of 0.3 μM in the focal volume. Fast acquisition with a dwell time of 0.1 ms implies a hundred times higher detection limit.

The sensitivity limit for PbS CQDs is one order of magnitude higher than what we obtained for CdSe/ZnS CQDs (10 CQDs per $\sqrt{\text{Hz}}$) in our previous work.[11,12] Different aspects have to be considered to understand this difference.

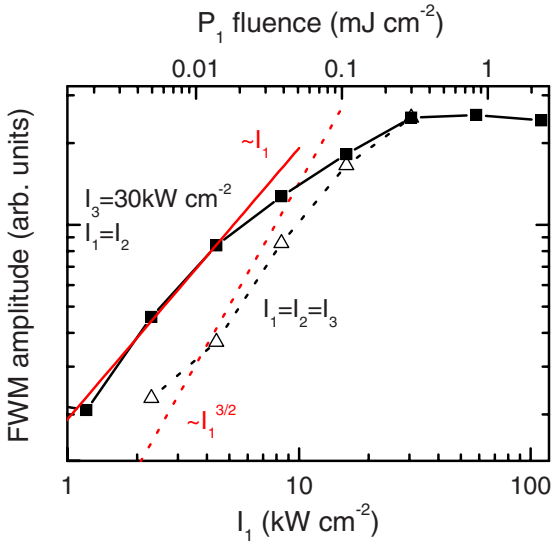

FIG. 3. (Color online) Dependence of the FWM amplitude on the intensity of $P_1(I_1)$, for equal intensities of the three fields (triangles) and for $I_1=I_2$ and constant intensity of the third beam $I_3=30$ kW/cm^2 (squares). The solid (dashed) line shows a third-order nonlinearity scaling for equal excitation intensities of the two (three) fields. The excitation wavelength is 1.25 μm.

The first one is the exciton lifetime. From the integrated extinction coefficient,[29] the radiative lifetime in PbS CQDs is 64 times longer compared to CdSe/ZnS CQDs, consistent with measured lifetimes of 1–2 μs in PbS CQDs (Refs. 39 and 40) and 10–20 ns in CdSe/ZnS CQDs.[41,42] The laser repetition period used in our experiments (13 ns) is thus shorter than the radiative lifetime of PbS CQDs, and one would expect that in this case the signal should be reduced by the ratio between lifetime and repetition period due to accumulation effects. However, as shown in the next section we observe that the effect of carrier accumulation over the repetition period in PbS CQDs gives a contribution to the absorption bleaching of only 10%. This is attributed to a reduction in the exciton lifetime due to Auger recombination as discussed later. The lifetime effect can thus be neglected for the sensitivity. The second aspect is the fourfold increase in degeneracy in PbS compared to CdSe/ZnS, resulting in a saturation for absorption of four photons compared to one in CdSe/ZnS CQDs. Charging of the CQDs would reduce this factor due to Pauli blocking of some of the transitions. The third aspect is the ratio between the focus area and the absorption cross section per transition, giving the number of photons n_3 in the third pulse at saturation. The FWM field per absorbed/emitted photon scales as $1/\sqrt{n_3}$. The two times larger wavelength for the PbS CQDs increases the focus area by a factor of 4 while the absorption cross section per transition is $\sim$40 times smaller than in CdSe/ZnS CQDs. (We measured an extinction coefficient at the fundamental absorption peak wavelengths of $\sim 9\times 10^5$ M^{-1} cm^{-1} and $\sim 8.4\times 10^4$ M^{-1} cm^{-1} for CdSe/ZnS and PbS CQDs, respectively, in general agreement with literature values.[29,43–45]) Accordingly, the sensitivity limit is reduced by a factor of $\sim$13. Altogether, the different components result in a 3–13

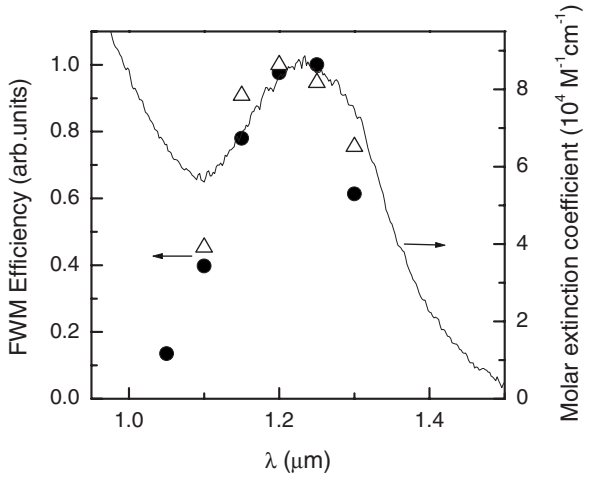

FIG. 4. Molar extinction coefficient of the sample (solid line) and FWM efficiency (dots) at low excitation as a function of excitation wavelength. The triangles show the saturated FWM amplitude for high excitation.

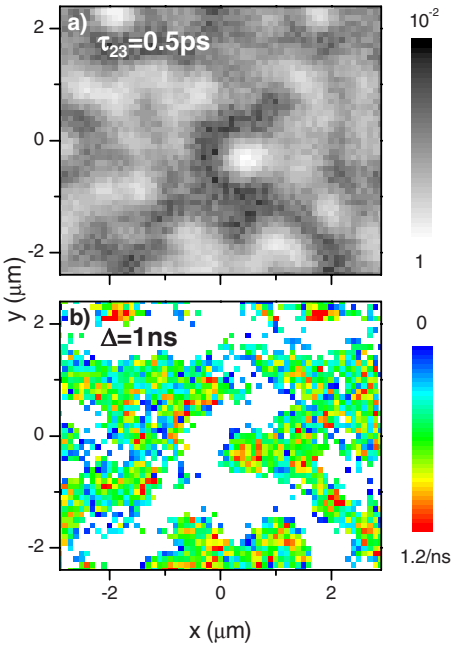

FIG. 5. (Color online) (a) FWM intensity *xy* scan for $\tau_{23}=0.5$ ps on 3.7 nm-PbS CQDs dispersed in a polystyrene layer. Logarithmic grayscale as indicated. (b) Average decay rate from $\tau_{23}=0.5$ ps to 1 ns (see text). Linear color scale as indicated. The excitation wavelength was 1.1 μm, resonant with the first absorption peak of the CQDs. $I_{tot}=17.7$ kW/cm^2 (77 μJ/cm^2 per pulse). Pixel size 0.1 μm.

times lower sensitivity for the PbS CQDs for a charging by 0–3 carriers, consistent with our measurement.

Besides detection sensitivity, issues to be considered for the applicability of PbS CQDs in bioimaging are their biocompatibility and photostability. The presence of the oleic acid capping in our samples prevents water solubility, but water soluble PbS CQDs have been demonstrated using ligand exchange,[46] or apoferritin encapsulation which also resulted in reduced cytotoxicity,[47] and allowed for deep *in vivo* tissue imaging based on luminescence from these CQDs.[48] While Peterson *et al.*[6] reported poor luminescence stability of PbS CQDs, we found no significant degradation in our samples which were synthesized via a different procedure.[9,29] More specifically, suspensions of PbS CQDs were stored for six weeks under ambient conditions and we did not observe a blueshift of the CQD absorption peak, which would indicate oxidation. Moving to PbS/CdS core/shell structures is expected to further improve the CQD stability. In the FWM imaging, we did not observe any irreversible decrease in the signal even after hours of illumination at excitation intensities up to 1 MW/cm^2.

To investigate the resonant nature of the FWM to the excitonic ground state absorption of the PbS CQDs, we have measured its dependence on the excitation wavelength λ in the range 1.05–1.3 μm in the low excitation regime (I_{tot} ~6 kW/cm^2). To remove the effect of changing excitation power, detection efficiency, and focus size, we define the FWM efficiency,

$$\epsilon_{FWM} = \frac{E_{FWM}}{\sqrt{p_1 p_2 p_3}}, \quad (1)$$

where E_{FWM} is the measured FWM amplitude corrected for the wavelength dependence of the detection efficiency, and $p_{1,2,3}$ are the excitation powers of the three excitation beams.[49] In this way, ϵ_{FWM} is given by the effective third-order susceptibility of the QDs. The measured ϵ_{FWM} is shown in Fig. 4 (dots) as a function of the excitation wavelength, together with the spectrum of the molar extinction coefficient of the sample (solid line). The FWM efficiency has its maximum for excitation resonant with the fundamental absorption peak, consistent with observations in CdSe/ZnS CQDs (Ref. 11) and similar to the nonlinear refractive index of PbSe CQDs measured with the Z-scan technique.[50] For excitation close to the first excited state (λ ~ 1.05 μm), a significant reduction is observed in the FWM efficiency despite a similar extinction coefficient. A shorter dephasing time and relaxation processes into the ground states are the likely origins of the reduced FWM efficiency in the excited states. The resonant behavior is also present in the saturated FWM amplitude at high excitation intensities I_{tot} ~300 kW/cm^2, shown also in Fig. 4. From the point of view of microscopy applications, the resonant nature of the measured FWM signal is allowing for multicolor FWM imaging where CQDs of different size/composition, and hence different ground-state excitonic absorption resonance, can be used to selectively tag different parts of a specimen.

Three-beam transient FWM gives access to the exciton population dynamics, which is analyzed in the next section. Combined with microscopy, this enables the acquisition of a spatially resolved map of CQD carrier lifetime which could be used to distinguish different CQDs or the influence of the local environment (lifetime imaging), and an example of FWM lifetime imaging is shown in Fig. 5. The *xy* scan of the FWM intensity (I_{FWM}) acquired at $\tau_{23}=0.5$ ps is shown together with the quantity $r=-\{\ln[I_{FWM}(\tau_{23}+\Delta)/I_{FWM}(\tau_{23})]\}/\Delta$ which gives the average decay rate of the FWM intensity over the time interval Δ starting at τ_{23}. Here

we show data for $\Delta=1$ ns. A spatially resolved distribution of decay rates is observed with a different pattern compared to the intensity, showing that the lifetime can give an additional contrast channel. Future development of CQDs with lifetimes depending on the chemical environment, such as the pH value, can render this contrast technique useful, similar to fluorescence lifetime imaging modalities. In this respect, charging-induced lifetime reduction could be a relevant transduction mechanism.

B. Dynamics

Besides imaging applications, transient FWM in a three-beam geometry is a known method to directly measure the excitonic population dynamics with pump and probe pulses resonant to the same transition, as also recently demonstrated by us on InAs/GaAs quantum dots.[28] These dynamics reflect physical processes which are important, beyond fundamental interest, for applications in, e.g., photovoltaics and optoelectronics.[15–18,21–27,51,52] In Fig. 6, the dependence of the FWM amplitude on τ_{23} is shown on 4.4 nm PbS CQDs for two excitation wavelengths, either resonant with the excitonic ground state (upper curves) or closer to the first excited state (lower curve).

We found that to fit the FWM dynamics a minimum of three different exponential decays plus an offset are needed to result in a residual comparable to the noise. The offset is due to the carrier accumulation over the pulse sequence from lifetimes longer than the repetition rate of the pulsed laser. We also found that good fits to the dynamics for all excitation intensities can be obtained fixing the time constants (see Fig. 6) and using only the amplitudes as fitting parameters. The dependence of the resulting amplitudes on the total excitation intensity (equal intensities on each beam) is shown in Fig. 7.

We first discuss the dynamics for excitation in resonance with the excitonic ground-state transition. The components with 11 and 125 ps time constants have amplitudes which are scaling slightly superlinearly with intensity while the 2.8 ns component scales slightly sublinearly. We estimated the number of photogenerated excitons per repetition from the absorption cross section and the excitation fluence at constructive interference of P_1 and P_2. This number reaches about unity for the maximum excitation intensity used (see scale in Fig. 7). The corresponding probabilities to create a biexciton or a triexciton according to the Poisson distribution of absorbed photons are given for comparison. Since all observed amplitudes scale approximately linearly with the excitation intensity (see dotted line in Fig. 7), similar to the total number of excited excitons, we do not have clear evidence of biexciton or multiexciton Auger recombination of carriers excited in a single repetition. However, we cannot exclude processes due to accumulation of excitons or charges with lifetimes longer than the pulse repetition rate. The resulting charged exciton and biexciton processes could show a close to linear dependence with the single pulse excitation intensity. In the literature, nonresonant pump-probe experiments show that charged exciton and biexciton Auger recombination occur with time constants of 10–100 ps for CQDs

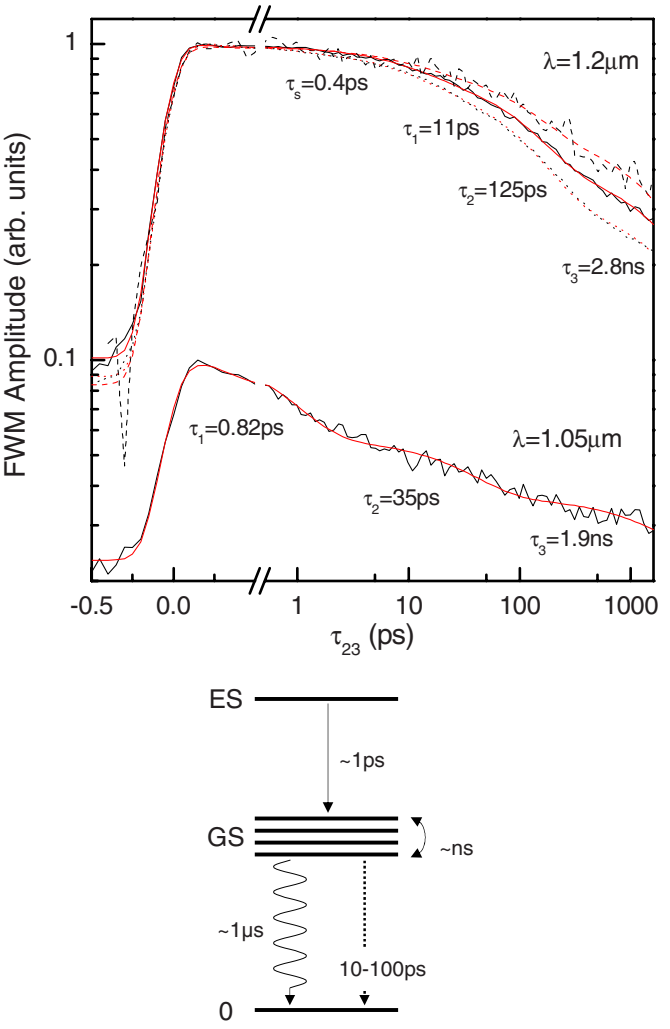

FIG. 6. (Color online) Top: dynamics of the FWM amplitude versus τ_{23} for two different excitation wavelengths as indicated. The curves are vertically displaced for clarity. The total excitation intensities (equal intensities on each beam) for $\lambda=1.2$ μm are 2.6 (dashed line), 11 (solid line), and 22 kW/cm^2 (dotted line), and 23 kW/cm^2 for $\lambda=1.05$ μm. The red lines are fits to the data. The obtained time constants are given. The fast time constant $\tau_s=0.4$ ps is observed only for the highest excitation at $\lambda=1.2$ μm. Bottom: a sketch of the excitonic level structure with the possible transitions related to the observed dynamics is shown. GS: exciton ground state, ES: exciton excited state. Wavy (straight) lines represent radiative (phonon-assisted) processes. The dashed line represents charged exciton and biexciton Auger recombination processes.

with size similar to the ones investigated here.[16,53] Hence it is likely that the processes with time constants in the range 10–100 ps observed in the FWM dynamics are due to Auger recombination of charged excitons and biexcitons mediated by carrier accumulation. The contribution associated to multiexcitonic recombination in absence of carrier accumulation can be calculated from Poisson's distribution. We find that these processes should contribute to 30–40 % of the total signal for $\langle N_{ex}\rangle=0.75$. The measured weight of the 11 and 125 ps processes add to 60% of the total signal at this $\langle N_{ex}\rangle$, indicating that in the experiment there are additional contributions due to carrier accumulation. However, the uncer-

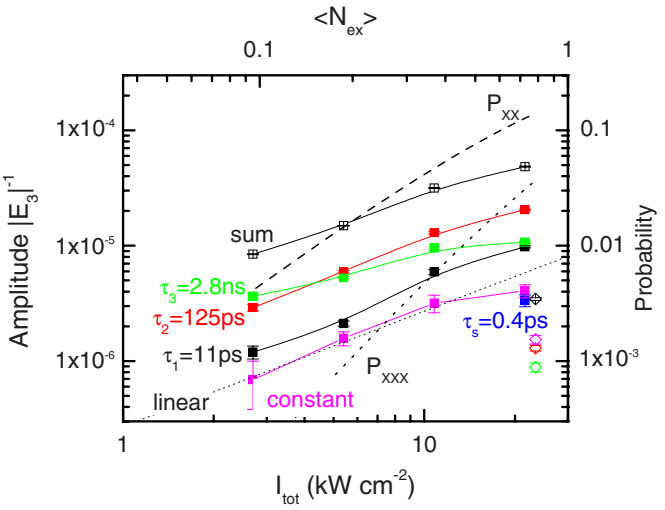

FIG. 7. (Color online) Amplitudes of the decay processes obtained from the fits divided by the field amplitude of the third pulse (full squares) as a function of the total excitation intensity for $\lambda = 1.2$ μm, and for a fixed $I_{tot} = 23$ kW/cm^2 at $\lambda = 1.05$ μm (empty diamonds). The empty squares represent the sum of the amplitudes at $\lambda = 1.2$ μm. Probabilities of creating a biexciton (dashed line) or a triexciton (dotted line) by the pump pulses according to Poisson's distribution are shown. $\langle N_{ex} \rangle$ is the average number of photogenerated excitons per dot at constructive $P_{1,2}$ interference for excitation at 1.2 μm. The dotted thin line shows a linear dependence on the total excitation intensity.

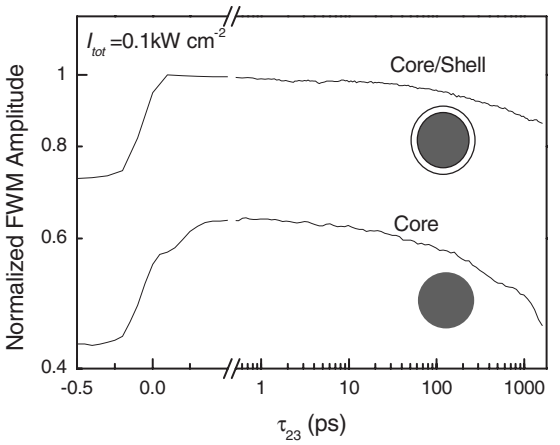

FIG. 8. Dynamics of the FWM amplitude signal versus τ_{23} for core-only PbS (bottom) and core/shell PbS/CdS (top) CQDs for very low excitation intensities of $I_{tot} = 0.1$ kW/cm^2. The excitation wavelength (1.3 μm) is resonant with the fundamental absorption peaks. The curves are vertically displaced for clarity.

tainty in the estimate of $\langle N_{ex} \rangle$ and the lack of knowledge about the carrier accumulation processes prevent a more quantitative analysis.

Turning now to the nanosecond dynamics, we note that Auger recombination processes on this time scale have not been reported in literature. We observe that this dynamics persists in our resonant FWM experiment even at very low excitation intensities ($I_{tot} = 0.1$ kW/cm^2) for which the 10–100 ps processes are virtually absent. We also performed a comparison between core-only PbS CQDs and core/shell PbS/CdS CQDs of similar core size and 0.44 nm shell thickness, which are expected to be more photostable and exhibit less influence of surface defects owing to the presence of the shell (see Fig. 8). We found that the dynamics at low excitation intensity is similar between the two samples, with the nanosecond time constant being somewhat longer (2.7 ns compared to 1.2 ns) and the constant term having a slightly larger weight in the core/shell dots (73% compared to 67%) while the 10–100 ps processes are weak with less than 5%. This behavior further supports the attribution of the 10–100 ps processes to Auger recombination of charged excitons and biexcitons while the nanosecond and longer lived contributions are more likely related to single exciton dynamics. The constant term accounting for ~70% of the total signal at low intensity is expected from the long excitonic lifetime compared to the repetition rate. We note that 0.1 kW/cm^2 excitation corresponds to only 0.36% population of the exciton ground state per repetition, which results in ~8% steady-state population considering the 76 MHz repetition rate and an exciton lifetime of ~300 ns (as measured by us in the core-only sample in a time-resolved photoluminescence experiment at 500 kHz repetition rate). Hence at this low excitation, the probability of multiexciton occupation should be negligible. A possible origin of the nanosecond component could be exciton relaxation into trap states. However density-functional calculations[54] show the absence of trap states in the CQD gap, which was confirmed experimentally in photoluminescence measurements.[55] Furthermore, the similar dynamics of core-only and core-shell structures indicates that there are no relevant surface trap states, as they are expected to be suppressed by the shell. If relaxation through defect states is ruled out, an intrinsic mechanism for the nanosecond dynamics is phonon-assisted thermalization between the set of eight S-like exciton ground states (see sketch of Fig. 6). The different S-like ground states have different energies and oscillator strength due to intervalley and interband coupling and Coulomb and exchange interactions.[14] Therefore, after resonant excitation which populates states proportionally to their oscillator strength, a thermalization between the states results in a reduced absorption bleaching, as density is transferred away from the large oscillator strength transitions.

When varying the excitation wavelength, no significant difference in the dynamics was observed from 1.3 to 1.1 μm while an additional component of ~1 ps time constant was found at 1.05 μm, which is close to the first P-like excited-state transition [see Fig. 1(b)]. This component was scaling linear with the excitation intensity, and can be attributed to exciton thermalization from the P excited states to the S ground states (see sketch in Fig. 6), consistent with 1P-1S relaxation rates reported in the literature.[56]

IV. CONCLUSION

We have demonstrated that PbS colloidal quantum dots absorbing in the near infrared can be imaged with high spatial resolution and intrinsic optical sectioning, using a coherent multiphoton microscopy technique based on transient resonant four-wave mixing. Since this detection is not based

on fluorescence, it overcomes limitations associated with fluorescence photobleaching or blinking and is not affected by the high level of detector noise in the near infrared, hence representing an alternative to two-photon fluorescence microscopy. We demonstrated the resonant behavior of the four-wave-mixing nonlinearity, promising for multicolor imaging of quantum dots absorbing at different wavelengths. The potential of lifetime imaging enabled by the time-resolved detection of the carrier density was also shown. The dynamics of the absorption recovery in resonance with the excitonic ground state was interpreted in terms of charged exciton and biexciton Auger recombination in the 10–100 ps time scale, phonon-assisted thermalization between the different excitonic ground states in the nanosecond time scale, and exciton recombination in the microsecond time scale.

ACKNOWLEDGMENTS

F.M. acknowledges funding from the European Community's Seventh Framework Program (FP7/2007-2013) under grant Agreement No. PIEF-GA-2008-220901. W.L. and P.B. acknowledge the EPSRC (Grant No. EP/E0131198/1) UK Research Council for financial support. I.M. is a researcher with the FWO-Vlaanderen. This project is funded by the Belgian Science Policy Office (Grant No. IAP P6/10) and the FWO-Vlaanderen (Grant No. G.0.144.08).

*masiaf@cf.ac.uk

[1] P. Lodahl, A. Floris van Driel, I. S. Nikolaev, A. Irman, K. Overgaag, D. Vanmaekelbergh, and W. L. Vos, Nature (London) **430**, 654 (2004).
[2] See references in Nat. Photonics **3**(6), 305 (2009).
[3] X. Michalet, F. F. Pinaud, L. A. Bentolila, J. M. Tsay, S. Doose, J. J. Li, G. Sundaresan, A. M. Wu, S. S. Gambhir, and S. Weiss, Science **307**, 538 (2005).
[4] D. Larson, W. Zipfel, R. Williams, S. Clark, M. Bruchez, F. Wise, and W. Webb, Science **300**, 1434 (2003).
[5] M. Bruchez, Jr., M. Moronne, P. Gin, S. Weiss, and A. P. Alivisatos, Science **281**, 2013 (1998).
[6] J. J. Peterson and T. D. Krauss, Nano Lett. **6**, 510 (2006).
[7] C. M. Evans, L. Guo, J. J. Peterson, S. Maccagnano-Zacher, and T. D. Krauss, Nano Lett. **8**, 2896 (2008).
[8] H. Du, C. Chen, R. Krishnan, T. D. Krauss, J. M. Harbold, F. W. Wise, M. G. Thomas, and J. Silcox, Nano Lett. **2**, 1321 (2002).
[9] L. Cademartiri, E. Montanari, G. Calestani, A. Migliori, A. Guagliardi, and G. A. Ozin, J. Am. Chem. Soc. **128**, 10337 (2006).
[10] J. M. Pietryga, R. D. Schaller, D. Werder, M. H. Stewart, V. I. Klimov, and J. A. Hollingsworth, J. Am. Chem. Soc. **126**, 11752 (2004).
[11] F. Masia, W. Langbein, and P. Borri, Appl. Phys. Lett. **93**, 021114 (2008).
[12] F. Masia, W. Langbein, and P. Borri, Phys. Status Solidi C **6**, 916 (2009).
[13] W. Min, S. Lu, S. Chong, R. Roy, G. R. Holtom, and X. S. Xie, Nature (London) **461**, 1105 (2009).
[14] J. M. An, A. Franceschetti, and A. Zunger, Nano Lett. **7**, 2129 (2007).
[15] R. D. Schaller, M. Sykora, J. M. Pietryga, and V. I. Klimov, Nano Lett. **6**, 424 (2006).
[16] J. A. McGuire, J. Joo, J. M. Pietryga, R. D. Schaller, and V. I. Klimov, Acc. Chem. Res. **41**, 1810 (2008).
[17] R. D. Schaller and V. I. Klimov, Phys. Rev. Lett. **92**, 186601 (2004).
[18] R. J. Ellingson, M. C. Beard, J. C. Johnson, P. Yu, O. I. Micic, A. J. Nozik, A. Shabaev, and A. L. Efros, Nano Lett. **5**, 865 (2005).
[19] G. Nair, S. M. Geyer, L.-Y. Chang, and M. G. Bawendi, Phys. Rev. B **78**, 125325 (2008).
[20] J. Pijpers, R. Ulbricht, K. Tielrooij, A. Osherov, Y. Golan, C. Delerue, G. Allan, and M. Bonn, Nat. Phys. **5**, 811 (2009).
[21] J. M. Luther, M. C. Beard, Q. Song, M. Law, R. J. Ellingson, and A. J. Nozik, Nano Lett. **7**, 1779 (2007).
[22] M. T. Trinh, A. J. Houtepen, J. M. Schins, T. Hanrath, J. Piris, W. Knulst, A. P. L. M. Goossens, and L. D. A. Siebbeles, Nano Lett. **8**, 1713 (2008).
[23] M. Ji, S. Park, S. T. Connor, T. Mokari, Y. Cui, and K. J. Gaffney, Nano Lett. **9**, 1217 (2009).
[24] B. L. Wehrenberg, C. Wang, and P. Guyot-Sionnest, J. Phys. Chem. B **106**, 10634 (2002).
[25] J. M. Harbold, H. Du, T. D. Krauss, K.-S. Cho, C. B. Murray, and F. W. Wise, Phys. Rev. B **72**, 195312 (2005).
[26] E. Istrate, S. Hoogland, V. Sukhovatkin, L. Levina, S. Myrskog, P. W. E. Smith, and E. H. Sargent, J. Phys. Chem. B **112**, 2757 (2008).
[27] J. M. Pietryga, K. K. Zhuravlev, M. Whitehead, V. I. Klimov, and R. D. Schaller, Phys. Rev. Lett. **101**, 217401 (2008).
[28] M. P. Lumb, E. Clarke, E. Harbord, P. Spencer, R. Murray, F. Masia, P. Borri, W. Langbein, C. G. Leburn, C. Jappy, N. K. Metzger, C. T. A. Brown, and W. Sibbett, Appl. Phys. Lett. **95**, 041101 (2009).
[29] I. Moreels, K. Lambert, D. Smeets, D. De Muynck, T. Nollet, J. C. Martins, F. Vanhaecke, A. Vantomme, C. Delerue, G. Allan, and Z. Hens, ACS Nano **3**, 3023 (2009).
[30] J. M. Pietryga, D. J. Werder, D. J. Williams, J. L. Casson, R. D. Schaller, V. I. Klimov, and J. A. Hollingsworth, J. Am. Chem. Soc. **130**, 4879 (2008).
[31] K. Lambert, B. De Geyter, I. Moreels, and Z. Hens, Chem. Mater. **21**, 778 (2009).
[32] I. Moreels, B. De Geyter, D. Van Thourhout, and Z. Hens, J. Opt. Soc. Am. B **26**, 1243 (2009).
[33] F. Masia, W. Langbein, P. Watson, and P. Borri, Opt. Lett. **34**, 1816 (2009).
[34] P. Borri and W. Langbein, J. Phys.: Condens. Matter **19**, 295201 (2007).
[35] J. Shah, *Ultrafast Spectroscopy of Semiconductors and Semiconductor Nanostructures* (Springer, Berlin, 1996), Chap. 2.
[36] H. Kamisaka, S. V. Kilina, K. Yamashita, and O. V. Prezhdo, Nano Lett. **6**, 2295 (2006).
[37] E. O. Potma, W. P. de Boeij, and D. A. Wiersma, J. Opt. Soc. Am. B **17**, 1678 (2000).
[38] J. M. Squirrell, D. L. Wokosin, J. G. White, and B. D. Bavister, Nat. Biotechnol. **17**, 763 (1999).

[39] J. H. Warner, E. Thomsen, A. R. Watt, N. R. Heckenberg, and H. Rubinsztein-Dunlop, Nanotechnology **16**, 175 (2005).
[40] L. Cademartiri, J. Bertolotti, R. Sapienza, D. S. Wiersma, G. von Freymann, and G. A. Ozin, J. Phys. Chem. B **110**, 671 (2006).
[41] S. J. Lim, B. Chon, T. Joo, and S. K. Shin, J. Phys. Chem. C **112**, 1744 (2008).
[42] M. Jones, S. S. Lo, and G. D. Scholes, J. Phys. Chem. C **113**, 18632 (2009).
[43] C. A. Leatherdale, W.-K. Woo, F. V. Mikulec, and M. G. Bawendi, J. Phys. Chem. B **106**, 7619 (2002).
[44] L. Q. W. William Yu, W. Guo, and X. Peng, Chem. Mater. **15**, 2854 (2003).
[45] I. Moreels, Ph.D. thesis, Gent University, 2009.
[46] B.-R. Hyun, H. Chen, D. A. Rey, F. W. Wise, and C. A. Batt, J. Phys. Chem. B **111**, 5726 (2007).
[47] L. Turyanska, T. D. Bradshaw, J. Sharpe, M. Li, S. Mann, N. R. Thomas, and A. Patanè, Small **5**, 1738 (2009).
[48] L. Turyanska, O. Makarovsky, U. Elfurawi, M. W. Fay, J. W. Bowers, H. M. Upadhyaya, M. Li, S. Mann, N. R. Thomas, and A. Patanè (unpublished).
[49] The variation in the FWM amplitude due to the change in the focal volume for different wavelengths is compensated by the increase in the number of QDs in the focal volume.
[50] I. Moreels, Z. Hens, P. Kockaert, J. Loicq, and D. Van Thourhout, Appl. Phys. Lett. **89**, 193106 (2006).
[51] K. Wundke, S. Pötting, J. Auxier, A. Schülzgen, N. Peyghambarian, and N. F. Borrelli, Appl. Phys. Lett. **76**, 10 (2000).
[52] A. M. Malyarevich, M. S. Gaponenko, K. V. Yumashev, A. A. Lagatsky, W. Sibbett, A. A. Zhilin, and A. A. Lipovskii, J. Appl. Phys. **100**, 023108 (2006).
[53] I. Robel, R. Gresback, U. Kortshagen, R. D. Schaller, and V. I. Klimov, Phys. Rev. Lett. **102**, 177404 (2009).
[54] A. Franceschetti, Phys. Rev. B **78**, 075418 (2008).
[55] M. J. Fernée, E. Thomsen, P. Jensen, and H. Rubinsztein-Dunlop, Nanotechnology **17**, 956 (2006).
[56] R. D. Schaller *et al.*, Phys. Rev. Lett. **95**, 196401 (2005).